Fukushima Dai-ichi fuel debris retrieval: CFD calculations of aerosol dispersion and mitigation by spray systems in representative conditions of the 1F2 reactor pedestal

Thomas Gelain, Emmanuel Porcheron, Yohan Leblois, Ioana Doyen, Christophe Journeau, Remi Delalez, Damien Roulet

DEM 2021 – International Conference on Decommissioning Challenges: Industrial Reality, Lessons learned and Prospects

France, Avignon – 2021, September 13 | 15

Fukushima Dai-ichi fuel debris retrieval: CFD calculations of aerosol dispersion and mitigation by spray systems in representative conditions of the 1F2 reactor pedestal

Thomas Gelain[1*], Emmanuel Porcheron[1], Yohan Leblois[1], Ioana Doyen[2], Christophe Journeau[3], Rémi Delalez[4], Damien Roulet[4]

[1]Institut de Radioprotection et de Sûreté Nucléaire (IRSN), PSN-RES, SCA, Gif-Sur-Yvette, 91192, France
[2]CEA, DEN, Saclay, DM2S/SEMT/LTA, Gif-Sur-Yvette, 91191, France
[3]CEA, DEN, Cadarache, SMTA/LPMA, St Paul lez Durance, 13108, France
[4]ONET, Engineering Business Unit, 26700, Pierrelatte, France
[*]Corresponding Author, E-mail: thomas.gelain@irsn.fr

KEYWORDS: *CFD, aerosol, dispersion, corium, laser cutting, Fukushima, pedestal*

Introduction

The general context of this study is related to demonstrate the feasibility of the use of the laser cutting technique for the fuel debris (or corium) retrieval on the damaged reactors of Fukushima Dai-ichi (1F). IRSN is involved in a project led by ONET Technologies, in collaboration with CEA, to bring relevant elements to analyse the risk occurred by the dispersion of aerosols emitted by the dismantling operations and to propose and evaluate solutions to mitigate this risk. This article will present CFD simulations of aerosols dispersion and removal by spray during the laser cutting phase in representative conditions of Fukushima Daiichi unit 2 (1F2) pedestal.

Study context and objectives

In the framework of the Fukushima subsidized projects of Decommissioning and Contaminated Water Management - Development of Fundamental Technologies for Retrieval of Fuel Debris and Internal Structures, CEA Saclay is performing a study on laser cutting process. IRSN has been assigned as a project subcontractor by ONET in order to realize experimental tests and simulations for characterizing airflows, aerosols emitted during laser cutting operations, and their dispersion and deposition in the DELIA laser cutting facility developed and operated by the CEA (ALTEA Platform) [1]. Several R&D projects have therefore been launched and subsidized by the Japanese government to study and prepare operations of the fuel debris retrieval. In this framework, a French consortium (ONET Technologies, CEA and IRSN) has been selected among others to implement R&D related to the laser cutting of fuel debris and to dust collection technology [1].
Different R&D tasks were proposed by IRSN to study aerosol issues during fuel debris removal by experimental and numerical means [2] [3] [4] [5] [6] . Among these tasks, one concerns more specifically the risk induced by the aerosol dispersion and deposition into the reactor during the laser cutting operations.
During the above-water cutting operations, particles will be produced, involving a potential risk of dispersion into the reactor pedestal and further into the environment in case of containment failure. In order to prevent and minimize this risk, different mitigation means were adapted and tested experimentally and numerically. Among them, the use of a spray for removing the airborne particles during dismantling operations was studied by IRSN, knowing that this mitigation means is considered as one of the best emergency system in nuclear reactors against several risks of dispersion of hazardous materials (hydrogen, radioactive aerosols) and allowing to avoid a severe accident but also the release of fission products into the environment.
In order to ensure an optimal use of this means in the Primary Containment Vessel (PCV), experiments and CFD simulations were performed in parallel way in order to evaluate the collection efficiency of this technique in the conditions of laser cutting and its applicability in a geometry representative of the reactor pedestal of the unit 2 of Fukushima Daiichi (1F2).
Different scales were used for this evaluation in order to ensure first the control of the environment and the associated measurement, and second to get enough data for the CFD code validation [7] [8].
Then, CFD calculations were carried out, on the basis of the optimum spray characteristics and of the numerical spray model validation, in a geometry as close as possible to the 1F2 reactor pedestal.

This article presents these simulations and the models implemented to take into account the interactions between the sprays and the aerosols.

Implemented models description

The CFD simulations of particle collection by spray were performed with the CFD code ANSYS CFX. In this context, the spray was simulated with a Lagrangian method whereas the particles, considered as polydispersed, were modelled with a simplified class method (no interaction between classes).
In order to take into account the particle scavenging by the spray, a collection efficiency model was implemented by following the methodology described by Plumecocq [9]. The particle collection mass flux, depending on the spray droplet and the particles characteristics, was implemented as a sink term in the transport equations for each class of particle.
The equations to be solved in the general case of a multicomponent mixture in turbulent flow and weakly compressible are as follows:

$$\frac{\partial \rho}{\partial t} + \nabla.(\rho \bar{U}) = 0 \qquad \text{(continuity)} \qquad (1)$$

$$\frac{\partial \rho \bar{U}}{\partial t} + \nabla.(\rho \bar{U} \otimes \bar{U}) = -\nabla \bar{\bar{P}} + \nabla\left[\mu_{eff}(\nabla \bar{U} + (\nabla \bar{U})^T)\right] + \rho g \qquad \text{(momentum)} \qquad (2)$$

$$\frac{\partial \rho \bar{Y}_p}{\partial t} + \nabla.\left(\rho \bar{\bar{U}} \bar{Y}_p\right) = S_p \; avec \; \bar{\bar{U}} = \bar{U} + \overline{U_{s,p}} \qquad \text{(particle transport)} \qquad (3)$$

$$\overline{U_{s,p}} = \tau_p \left(g_i - \left(\frac{\partial \bar{U}_i}{\partial t} + \bar{U}_j \frac{\partial \bar{U}_i}{\partial x_j} \right) - \frac{1}{C_p} \left(D_B \delta_{ij} + D^t_{p,ij} \right) \frac{\partial C_p}{\partial x_i} \right) \qquad \text{(slip model developed at IRSN [10])} \qquad (4)$$

$$\rho = \frac{\bar{P} M}{RT} \qquad with \qquad \frac{1}{M} = \sum_{c=1}^{n} \frac{\bar{Y}_c}{M_c} \qquad \text{(ideal gas law)} \qquad (5)$$

with ρ the density of the gaseous mixture, $\bar{U}$ the mean component of the velocity vector, $\bar{\bar{P}} = \bar{P} + \frac{2}{3}\rho k$ the modified mean pressure, μ_{eff} the effective viscosity, g the gravity vector, Y_p the mean value of the particle mass fraction, S_p a potential source term, $\bar{Y}_{air}$ the mean value of the air mass fraction, $\overline{U_{s,p}}$ the particle slip velocity, τ_p the particle relaxation time, D_B the Brownian diffusion coefficient of the particles, $D^t_{p,ij}$ the turbulent diffusion tensor, C_p the particle mass concentration ($C_p = \rho Y_p$), n the number of gaseous species, M the mixture molar mass, T the temperature et R the ideal gas constant.

- **Aerosol deposition model**

The deposition model considered in these simulations was developed by Nerisson et al. [10] and implemented by IRSN in ANSYS CFX by the way of wall flux terms for each transport equation [11]. This model takes into account the major phenomena of deposition such as turbulent diffusion, gravitational settling and turbulent impaction, and is detailed below:

$$\varphi_d = v_d^+ u^* C_p \qquad (6)$$

$$v_d^+ = \frac{g^+.n}{1 - e^{(g^+.n) I_p}} \qquad (7)$$

$$I_p = \frac{\sigma_t}{\kappa} \ln y^+ + \lambda\left(Sc_B, \tau_p^+\right) \qquad (8)$$

$$\lambda\left(Sc_B, \tau_p^+\right) = \left[\frac{{\tau_p^+}^{2n}}{\omega^n} + \left(\frac{Sc_B^{-\lambda_1}}{\lambda_0}\right)^n\right]^{-1/n} \quad (9)$$

Where v_d^+ is the non-dimensional particle velocity, u^* is the friction velocity (m.s^{-1}), C_p is the particle mass concentration (kg.m^{-3}), g^+ is the non-dimensional gravity vector, $\boldsymbol{n}$ is the wall normal vector, σ_t is the turbulent Schmidt number, κ is the Von Karman constant ($\kappa = 0.41$), y^+ is the non-dimensional wall distance, Sc_B is the Brownian Schmidt number and τ_p^+ is the non-dimensional relaxation time. In these equations, some constants were defined such as: $n = 2$, $\omega = 1700$, $\lambda_0 = 17.5$ and $\lambda_1 = 2/3$ [10].

The mass concentration C_p is defined at the first point of the mesh element the closest to the wall and u^* is defined by: $u^* = \sqrt{\tau_w/\rho}$, with τ_w the wall shear stress and ρ the carrier gas density.

- **Spray model**

For collecting the aerosols dispersed in the vessel, the considered technology is the spray. Indeed, the spray allows the aerosol scavenging with an efficiency depending mainly on the aerosol size and depending also on the droplet size, droplet velocity, droplet concentration and atmosphere conditions.
The spray modelling was performed by using a Lagrangian method whose momentum equation for the droplets is presented below.

$$m_d \frac{dU_d}{dt} = \sum F_d \quad (10)$$

Where m_d is the droplet mass, U_d is the droplet velocity and F_d represents all the forces applied on the droplet; in our case, only the drag (F_D) and buoyancy (F_G) forces were taken into account and are described by the following equations:

$$F_D = \frac{1}{2} C_D \rho A_d U_s |U_s| \quad (11)$$

$$F_G = m_d g \quad (12)$$

Where C_D is the drag coefficient [13], A_d is the effective particle cross section, U_s is the droplet slip velocity and g is the gravity acceleration.
A classical 'Blob' primary breakup model was applied. This simple model, already present in ANSYS CFX, only needs to specify the liquid mass flowrate, the spray angle and the nozzle radius allowing to calculate the spray droplets velocities. The initial droplet diameter is considered equal to the nozzle diameter before being subjected to aerodynamic stress inducing secondary breakup. Hence, the TAB (Taylor Analogy Breakup [14]) secondary breakup model was then applied, allowing to evolve the spray droplet depending on the typical breakup regimes defined by the Weber number and so-called:

- vibrational regime (We < 12);
- bag regime (12 < We < 100);
- sheet stripping regime (100<We<350);
- catastrophic regime (We>350).

We remind that the gas Weber number is defined by:

$$\mathrm{We} = \frac{\rho \ U_s^2 d_d}{\sigma} \quad (13)$$

Where d_d is the droplet diameter (m) and σ the liquid surface tension (N.m^{-1})

- **Collection model**

In order to allow the aerosol scavenging by the spray, a source term was applied to the aerosol Eulerian phase by the way of a collection sink term added to the transport equation (3) of each particle class, in place of S_p. This sink term (S_{capt}) takes into account many variables depending on the spray, on the

aerosol and also on the collection efficiency. It is defined hereafter:

$$S_{capt} = E_m \pi r_p^2 U_d \frac{X_d}{V_d} C_p \quad (14)$$

Where E_m is the collection mechanical efficiency, r_p is the particle radius, U_d is the droplet velocity, X_d is the droplet volume fraction, V_d is the droplet volume and C_p is the particle mass concentration.
The mechanical efficiency can be defined by the contribution of different specific efficiencies:

$$E_m = 1 - \left(1 - E_{diff}\right)\left(1 - E_{int}\right)\left(1 - E_{imp}\right) \quad (15)$$

Where E_{diff}, E_{int} and E_{imp} are respectively the collection efficiencies by Brownian diffusion, interception and impaction. These different efficiencies are described in [7] and [9].

CFD Modeling

- **Geometry and calculation domain**

The geometry of the pedestal was designed from the picture presented in Figure 1 [15].

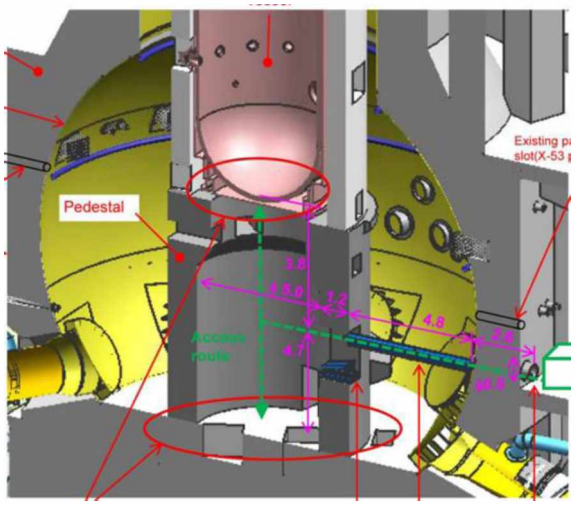

Figure 1: sketch of the 1F2 pedestal and its global dimensions [15]

A lot of pictures were taken inside the pedestal thanks to robots able to access the interior and allowing to get a global preview of the internal situation leading to obtain the current geometry of the pedestal with representativeness enough. Some documents were also used for that, especially those coming from IRID and TEPCO entitled "*Fukushima Daiichi Nuclear Power Station - Unit 2 Primary Containment Vessel Internal Investigation*" [16] and "*Unit 2 Primary Containment Vessel Investigation at Fukushima Daiichi Nuclear Power Station (By the self-propelled investigation device)*" [17]. In these documents, the state of the bottom of the pedestal is described and illustrated with pictures.
The global dimensions of the 1F2 pedestal are 5.0 m for the diameter and 8.5 m for the height. Three accesses were considered as mentioned in Figure 2: the worker access at the low level, the pedestal access at the median level and the CRD openings at the high level. Nonetheless, in order to avoid aerosol release outside the pedestal, these accesses were considered as closed with just diffuse leaks from outside towards inside (see Table 1).
In the previously cited documents, fuel debris deposits on the ground are evaluated in terms of thickness and locations allowing to design the scheme presented in Figure 2.

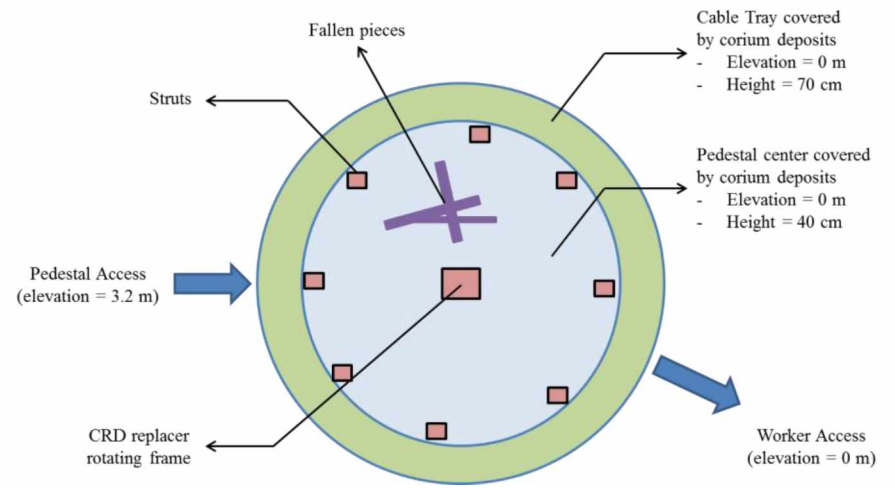

Figure 2: schematic design of the deposit configuration on the pedestal floor (top view)

As designed in Figure 2, a lot of elements are taken into account in this geometry in order to be the most representative of the real conditions of 1F2:

- a deposit height is considered on the pedestal floor. Thanks to the indications in the document [16], the deposits may be modelled by a layer of 40 cm in height in the center of the floor and a layer of 70 cm in height around the pedestal floor covering the cables tray;
- the struts which support the frame of the platforms are also designed with an arbitrarily evaluated cross section of 20 x 15 cm². Some fallen objects are deposited on the floor in order to represent a potential clutter.

The geometry of the pedestal for the computational domain is presented in Figure 3. All the elements detailed above are represented at the pedestal bottom except the Control Rod Drive (CRD) replacer, considering that it will be removed before starting fuel debris cutting operations in the pedestal.
CRD housings are also represented to be as close as possible to the real pedestal configuration. Indeed, the CRD housings are all represented (137) in order to take into account their clutter which may disturb the airflows in this area.

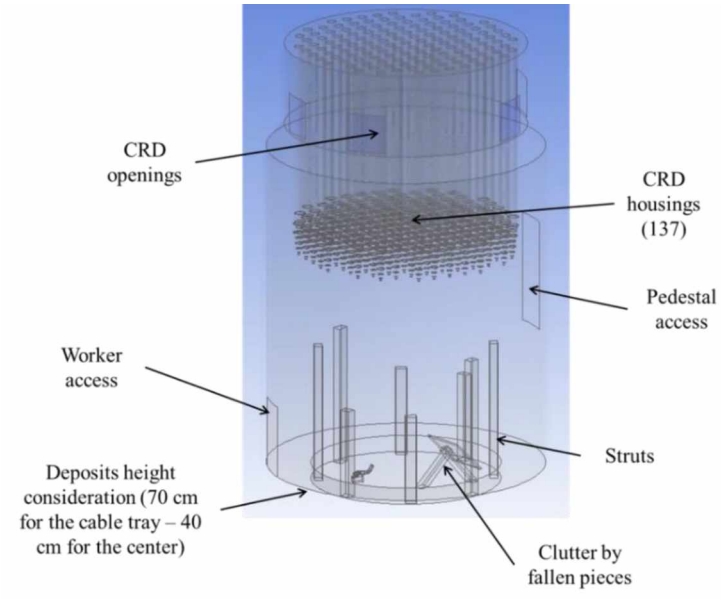

Figure 3: geometry of the pedestal

On the ground is also located the laser cutting head, the geometry of which is represented in Figure 4.

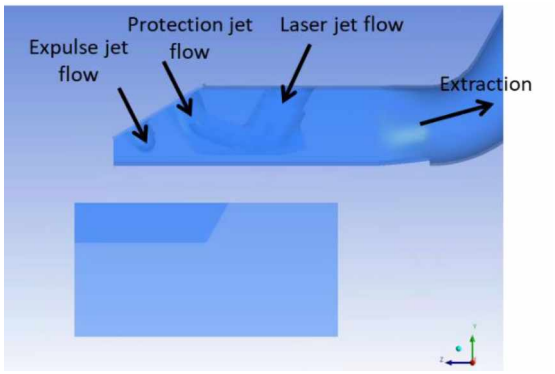

Figure 4: geometry of the laser cutting head, kerf and cut piece

The collection head allows to maintain the laser head during the cutting operations, but it aims also to collect the aerosols close to the emission source. For that, different gas jet flows are used and a duct allows the aerosol extraction:

- the laser jet flow is associated to the laser to confine the laser beam;
- the protection jet flow allows to protect the laser head from aerosols entry;
- the expulse jet flow allows the cleaning of the kerf performed by the laser and accumulation of molten fuel debris inside the kerf;
- the extraction allows to remove the airborne particles from the ambient. Indeed, the considered mitigation means for the cutting operations are this extraction close to the emission source coupled to local and global sprays, which are detailed thereafter.

- **Calculation setup**

Figure 5 and Figure 6 illustrate the location and the impact of the local and global sprays proposed to be implemented in the pedestal geometry. Their characteristics and locations were optimized by the way of the experimental validation and preliminary calculations.
The local spray is composed of two nozzles disposed on both sides of the cutting head. The nozzle characteristics are defined by a spray angle of 60° and a mass flow rate of 35 g/s.
The global spray is a spray bar located at 2.5 m above the floor. It includes 8 spray nozzles with a spray angle of 120° and a mass flow rate of 90 g/s, able to be embedded on the robot arm. That is why it can only be located at this height. As a consequence, only a quarter of the pedestal volume may be swept by this global spray, but it allows to better confine the aerosols produced by the cutting operations.

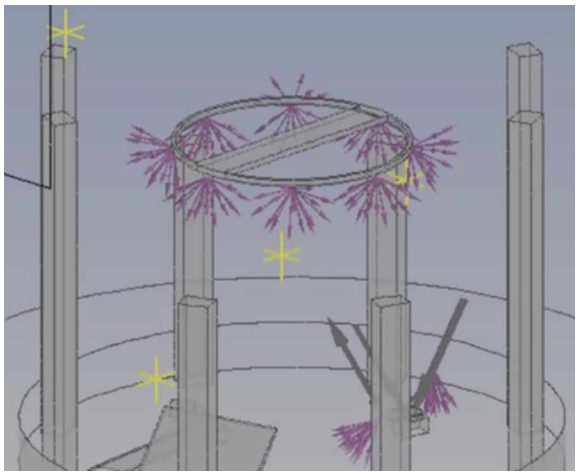

Figure 5: local and global sprays location inside the 1F2 pedestal

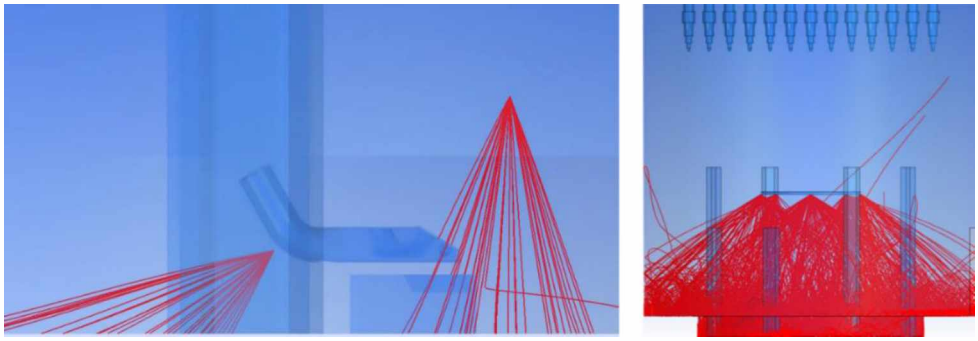

Figure 6: local and global spray impact

The calculations implemented for this first part, allowing the evaluation of the aerosols dispersion, are steady state calculations.
The input data and boundary conditions are summarized in Table 1.

Table 1: boundary conditions and input data

Boundary	Condition
Laser Head Conditions	
Laser jet flow	**Inlet (mass flow rate imposed)** Q_{inlet} = 400 l.min^{-1}, q_{inlet} = 0.007825 kg.s^{-1} $k = \frac{3}{2}(I\,U)^2, \varepsilon = C_\mu \rho \frac{k^2}{\mu_t}, \omega = \frac{\varepsilon}{k}$ $\mu_t = 1000 I\mu\,(I = 3.7\%)$
Expulse jet flow	**Inlet (mass flow rate imposed)** Q_{inlet} = 1600 l.min^{-1}, q_{inlet} = 0.0313 kg.s^{-1} $k = \frac{3}{2}(I\,U)^2, \varepsilon = C_\mu \rho \frac{k^2}{\mu_t}, \omega = \frac{\varepsilon}{k}$ $\mu_t = 1000 I\mu\,(I = 3.7\%)$
Protection jet flow	**Inlet (mass flow rate imposed)** Q_{inlet} = 1000 l.min^{-1}, q_{inlet} = 0.019562 kg.s^{-1} $k = \frac{3}{2}(I\,U)^2, \varepsilon = C_\mu \rho \frac{k^2}{\mu_t}, \omega = \frac{\varepsilon}{k}$ $\mu_t = 1000 I\mu\,(I = 3.7\%)$
Extraction	**Outlet (mass flow rate imposed)** Q_{outlet} = 200 m^3.h^{-1}, q_{outlet} = 0.065206 kg.s^{-1}
Aerosol injection in the kerf	**Wall (total source flux imposed)** q_{inj} = 10^{-5} kg.s^{-1}
Pedestal Conditions	
Walls	**Wall** No slip condition Automatic Wall law Aerosol sink flux φ_d
Openings (Worker Access, Pedestal Access, CRD Openings)	**Wall** No slip condition Automatic Wall law Leakage inflow φ_{in} = 0.0065208 kg.s^{-1}

It may be noticed in Table 1 that the aerosols are injected directly in the kerf as a source flux without velocity in order not to influence the flows induced by the laser head. The particle size distribution (PSD) of the injected aerosols corresponds to that measured experimentally during the cutting of ex-vessel simulant [18] and it is represented in Figure 7.

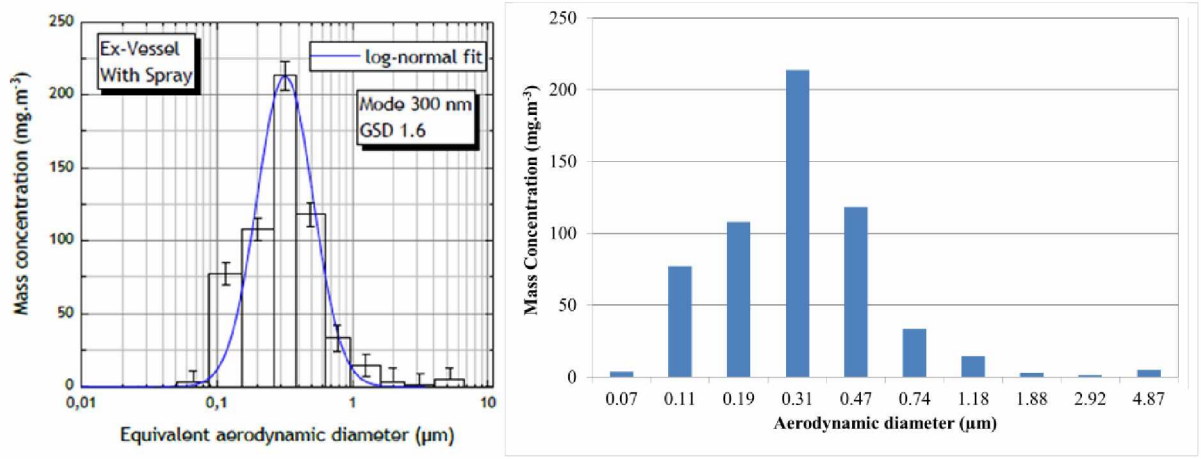

Figure 7: aerosol size distribution for ex-vessel simulant (experimental on the left – numerical on the right).

As shown in Figure 7 on the right, 10 classes were needed in order to well represent the experimental PSD. For that, ten variable transport equations similar to that detailed in equation (3) were implemented in ANSYS CFX.

Finally, the numerical parameters implemented for this calculation are gathered in Table 2.

Table 2: calculation parameters

Parameter	
Turbulence model	k-ω SST model (Shear Stress Transport)
Numerical scheme	Hybrid scheme (High Resolution)
Spray Model	Primary Breakup Model: Blob Secondary Breakup Model: TAB
Convergence	Steady state calculation
	Number of iterations = 15 000
	MAX residuals = 10^{-6}
Timescale	Between 0.01 s and 1 s

The following section presents the results obtained for this calculation in terms of global and separated efficiencies of particle collection, allowing to evaluate the remaining amount of aerosols dispersed inside the pedestal.

Results and discussion

This part presents the main results from the CFD calculations with an optimal configuration of the spray system evaluated in a preliminary parametric study. This study led to the needed to couple a local and a global spray in order to ensure a good confinement of the emitted particles.

The aim of these results is to show the capability of the mitigation means implemented in the geometry representative of the 1F2 reactor pedestal to limit the aerosol dispersion. For that, the global efficiency of each particle collection system was calculated by the way of the mass flow rates of the collected aerosols for each mitigation means divided by the injection mass flow rate. This calculation enables the evaluation of the spray and extraction collection efficiencies, the airborne particle loss due to deposition

and further the deduction of the part of dispersed aersols in the pedestal. These results are represented by a histogram in Figure 8.

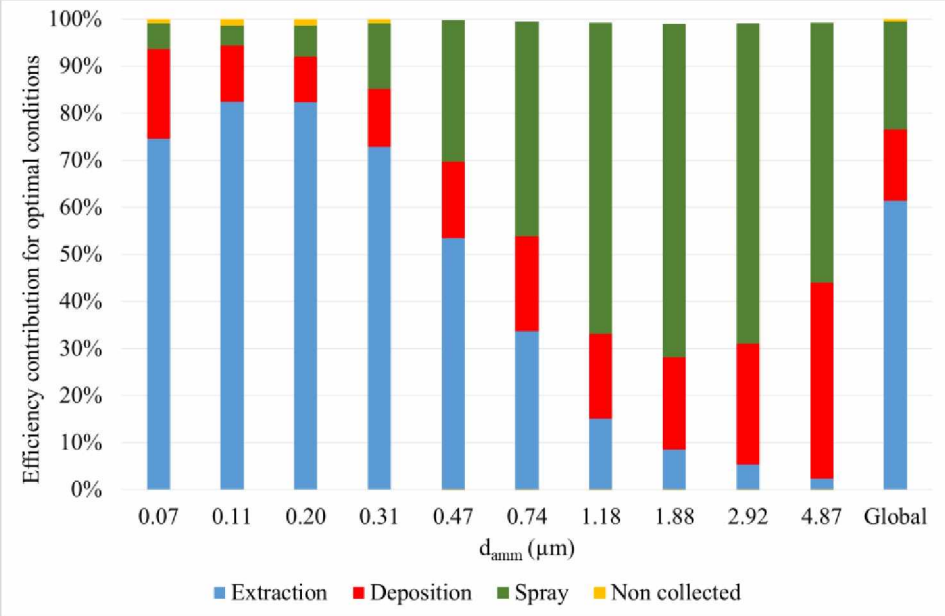

Figure 8: contribution of each collection means

These results bring a lot of information regarding the mitigation means whose mechanisms have been implemented in the calculation. Indeed, Figure 8 shows first the very good efficiency of the extraction system (blue rods) close to the emission source for aerosols smaller than 1 micron. It may be explained by the size of aerosols and their low Stokes number that involves they follow the airflows going to the extraction. On the opposite, aerosols bigger than 1 micron, leading to high Stokes number, cannot be collected with good efficiency by the extraction. However, they can be collected either by the local and global spray systems, or by deposition in majority on the ground by sedimentation or on the walls by impaction. This assumption is well represented in Figure 8 where the efficiency of the spray (green rods) increases strongly with the aerosol size and reaches a maximum for the diameter of 1.88 micron before decreasing due to the increase of the deposition contribution (red rods).
Furthermore, it may be observed that the deposition evolves in agreement with the classical deposition theory, with a minimum of deposition for an aerosol diameter between 0.2 and 0.31 micron, and a maximum of deposition for the biggest considered size of aerosols.

Since these efficiencies are known, it may be possible to deduce the part of aerosols dispersed in the pedestal. It is represented in Figure 8 by the yellow rods and it may be stated that this part is very low and especially notable for the smallest aerosols that are the most easily dispersible ones in the absence of mitigation.
What is the most remarkable in these results is the complementarity of all mitigation means (including the deposition), allowing to maintain a very high collection efficiency whatever the aerosol size, thus the PSD, and hence the cutting tools used for the dismantling operations generating various PSD [19].
This complementarity and the associated efficiency were evaluated for another PSD emitted by core boring mechanical cutting technique. This PSD was acquired experimentally during trials of core boring cutting and was implemented in the dataset of ANSYS CFX by considering the same injection configuration in order to be comparable with the laser cutting results. We are thus aware that the emission of this PSD is not fully representative of that by core boring but the objective is just to demonstrate the universality of this gathered mitigation means.

The PSD of the aerosols emitted by core boring cutting of Ex-vessel is presented in Figure 9 in comparison with that emitted by laser cutting of Ex-vessel. As shown, the two PSD are really different, with median diameter of 0.3 micron for laser cutting and around 4 microns for core boring cutting.
Hence, their behaviours in terms of dispersion, deposition and collection are totally different.

Figure 10 presents the results of the global efficiencies per mitigation means and shows that, as expected, the collection efficiency of the extraction close to the emission source is lower than for the PSD of aerosol emitted by laser cutting due to the bigger size of aerosols. However, for this aerosol diameter, the spray is much more efficient and is able to collect these aerosols. If we compare the contributions of each collection means for the complete PSD, the following tendencies are observed:

- the contribution of extraction is 60% for the laser cutting versus 6% for the core boring cutting;
- the contribution of spray is 23% for the laser cutting versus 51% for the core boring cutting.

These results highlight both the complementarity of the two studied mitigation means (extraction and spray) and their universality regarding the cutting tool used for the dismantling operations.

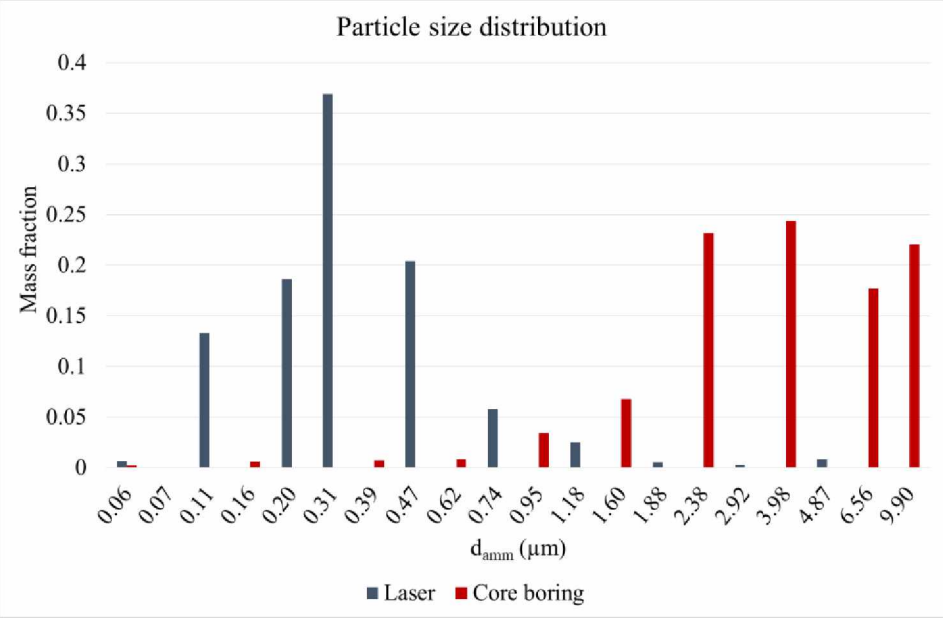

Figure 9: comparison of particle distributions of aerosols emitted by laser and core boring cutting techniques

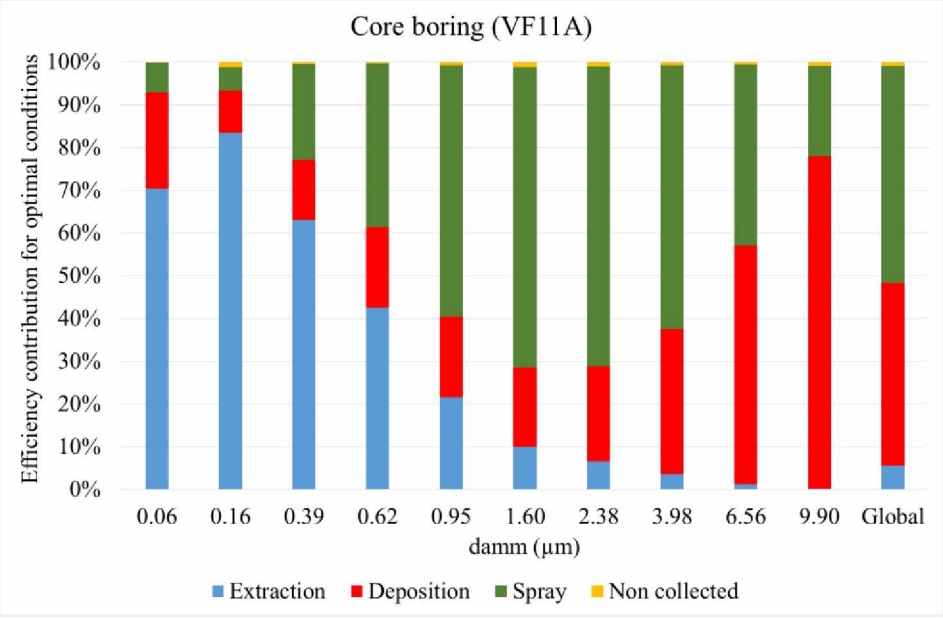

Figure 10: contribution of each collection means for core boring cutting of ex-vessel simulant

Conclusion

This article presents the results of CFD calculations on dispersion of aerosols emitted by cutting operations in a geometry representative of the 1F2 reactor pedestal.
The main issue of this study is to demonstrate the capabilities of the means developed and validated on small scale experiments to reach similar performance for the aerosol collection allowing to avoid their dispersion in the pedestal.
The considered mitigation means for the cutting operations are an extraction close to the emission source coupled to local and global sprays. Their collection efficiency was validated previously in experiments such as DELIA (CEA) or TOSQAN (IRSN), but also in CFD calculations [20].
In this article, this mitigation means are applied in a steady-state scenario of Ex-vessel aerosols emission and it is well shown that each of them is efficient for a specific aerosol diameter range, but also that they are complementary, which allows to cover a wide range of aerosol diameter with a global part of dispersed aerosols almost negligible. Nonetheless, it has to be noticed that the deposition is also important and contributes to limit the dispersion of aerosols in the pedestal.
This article showed also, as a consequence of this complementarity, the capability of the mitigation means to be adapted to different cutting tools that will produce different kinds of PSD in wide range of median diameters.

For the future, a transient scenario of cutting will be studied in order to be as close as possible to the real conditions of cutting and to evaluate the procedure to adopt on site in order to continuously maintain a low level of aerosols inside the pedestal.

References

[1] C. Chagnot, G. De Dinechin, and G. Canneau, "Cutting performances with new industrial continuous wave ND:YAG high power lasers: For dismantling of former nuclear workshops, the performances of recently introduced high power continuous wave ND:YAG lasers are assessed," *Nucl. Eng. Des.*, vol. 240, no. 10, pp. 2604–2613, 2010, doi: 10.1016/j.nucengdes.2010.06.041.

[2] T. Gelain, C. Chagnot, E. Porcheron, C. Journeau, S. Paul, and D. Roulet, "Development and validation of agglomeration model for CFD simulations of aerosol dispersion during Fukushima fuel debris retrieval," 2019.

[3] T. Gélain, E. Porcheron, C. Chagnot, and D. Roulet, "Numerical evaluation of the fate of aerosols produced by the laser cutting of Fukushima fuel debris simulants," 2018.

[4] T. Gelain, C. Chagnot, E. Porcheron, and D. Roulet, "CFD simulations of aerosol dispersion and agglomeration during the laser cutting of Fukushima fuel debris simulants," 2018.

[5] E. Porcheron, S. Peillon, T. Gélain, C. Chagnot, C. Journeau, and D. Roulet, "Analysis of aerosol emission and dispersion during the laser cutting of Fukushima fuel debris simulants," 2018.

[6] E. Porcheron, T. Gelain, C. Journeau, S. Peillon, and D. Roulet, "Analysis of Aerosol Emission and Dispersion During the Laser Cutting of Fukushima Fuel Debris Simulants," Aug. 2018, doi: 10.1115/ICONE26-81531.

[7] D. Marchand, E. Porcheron, P. Lemaitre, and G. Grehan, "Characterization of the washout of aerosols by spraying water for thermal hydraulic conditions representative of a severe accident in nuclear reactor containment," *10th Int. Conf. Liq. At. Spray Syst. ICLASS 2006*, 2006.

[8] E. Porcheron, C. Chagnot, Y. Leblois, C. Journeau, T. Gelain, and D. Roulet, "Study of spray scrubbing as mitigation means against aerosol dispersion during the Fukushima Dai-ichi fuel debris retrieval," *Int. Conf. Nucl. Eng. Proceedings, ICONE*, vol. 2019-May, 2019.

[9] William Plumecocq, "Etude de l'interaction d'un système d'aspersion liquide avec l'atmosphère environnante," 1997.

[10] P. Nerisson, O. Simonin, L. Ricciardi, A. Douce, and J. Fazileabasse, "Improved CFD transport and boundary conditions models for low-inertia particles," *Comput. Fluids*, vol. 40, no. 1, pp. 79–91, Jan. 2011, doi: 10.1016/j.compfluid.2010.08.013.

[11] T. Gélain, E. Porcheron, C. Chagnot, I. Doyen, C. Journeau, and D. Roulet, "Development and validation of an agglomeration model for CFD simulations of aerosol dispersion in the frame of Fukushima fuel debris retrieval," *J. Nucl. Sci. Technol.*, vol. 58, no. 6, pp. 690–703, 2021, doi: 10.1080/00223131.2020.1862717.

[12] "ANSYS CFX-Solver Theory Guide," no. January, 2017.

[13] L. Schiller and A. Naumann, "A drag coefficient correlation," *Zeitschrift des Vereins Dtsch. Ingenieure*, vol. 77, pp. 318–320, 1935.

[14] P. J. O'Rourke and A. A. Amsden, "The Tab Method for Numerical Calculation of Spray Droplet Breakup," *SAE*, 1987.

[15] S. Suzuki, "Demolition and Removal of Structures Damaged or Contaminated as a Result of the Fukushima Accident.," 2018.

[16] I. Tokyo Electric Power Company Holdings, "Fukushima Daiichi Nuclear Power Station Unit 2 Primary Containment Vessel Internal Investigation," 2018. [Online]. Available: https://www.tepco.co.jp/en/nu/fukushima-np/handouts/2018/images/handouts_180426_02-e.pdf.

[17] I. Tokyo Electric Power Company Holdings, "Unit 2 Primary Containment Vessel Investigation at Fukushima Daiichi Nuclear Power Station (By the self-propelled investigation device)," 2017. [Online]. Available: https://www.tepco.co.jp/en/nu/fukushima-np/handouts/2017/images/handouts_170202_01-e.pdf.

[18] E. Porcheron *et al.*, "Fukushima Daiichi fuel debris retrieval: results of aerosol characterization during non-radioactive simulants laser cutting," *J. Nucl. Sci. Technol.*, 2020.

[19] E. Porcheron, S. Bourrous, S. Peillon, C. Chagnot, C. Journeau, and D. Roulet, "Study of the influence of cutting tools on aerosol emission in the framework of Fukushima fuel debris retrieval," *Int. Top. Work. Fukushima Decommissioning Res. FDR2019*, 2019.

[20] H. Sun, Y. Leblois, T. Gelain, and E. Porcheron, "Experimental study on aerosol collection by spray droplets: Application to fission products removal in containment," *Int. Conf. Nucl. Eng. Proceedings, ICONE*, vol. 3, p. 1088863, 2020, doi: 10.1115/icone2020-16857.